

Supporting Information

**Strictly linear trinuclear Dy-Ca/Mg-Dy single-molecule magnets:
the impact of long-range f-f ferromagnetic interactions on
suppressing quantum tunnelling of magnetization leading to slow
magnetic relaxation**

Wan-Ying Zhang,^a Yong-Mei Tian,^a Hong-Feng Li,^a Peng Chen,^a Yi-Quan Zhang,^{b,*} Peng-Fei Yan^{a,*} and Wen-Bin Sun,^{a,*}

^a. Key Laboratory of Functional Inorganic Material Chemistry Ministry of Education, Heilongjiang University, Harbin 150080, P. R. China. E-mail: wenbinsun@126.com and yanpf@vip.sina.com

^b. Jiangsu Key Laboratory for NSLSCS, School of Physical Science and Technology, Nanjing Normal University, Nanjing 210023, P. R. China. E-mail: zhangyiquan@njnu.edu.cn

Table S1. Crystallographic details for complexes **1-4**.

	1	2	3	4
Empirical formula	C ₇₆ H ₅₈ CaDy ₂ N ₈ O ₉	C ₇₄ H ₅₀ Cl ₆ Dy ₂ MgN ₈ O ₈	C ₇₄ H ₅₀ CaCl ₆ Er ₂ N ₈ O ₈	C ₇₄ H ₅₀ Cl ₆ Er ₂ MgN ₈ O ₈
FW (g mol ⁻¹)	1592.38	1741.23	1766.52	1750.75
Crystal system	triclinic	triclinic	monoclinic	triclinic
Space group	P $\bar{1}$	P $\bar{1}$	P2 ₁ /c	P $\bar{1}$
Temperature (K)	293(2)	293(2)	293(2)	150.0(1)
<i>a</i> (Å)	11.8150(5)	10.2279(7)	29.7835(16)	10.1439(3)
<i>b</i> (Å)	12.3837(6)	13.4825(10)	23.1277(18)	13.3287(5)
<i>c</i> (Å)	14.0362(5)	14.1721(10)	10.3592(6)	14.0637(5)
α (°)	97.094(3)	111.287(7)	90	111.007(4)
β (°)	114.133(4)	106.541(6)	92.992(5)	106.679(3)
γ (°)	112.036(4)	90.335(6)	90	90.302(3)
<i>V</i> (Å ³)	1641.58(14)	1732.5(2)	7125.9(8)	1687.94(11)
ρ_{calcd} (Mg m ⁻³)	1.611	1.669	1.647	1.722
μ (mm ⁻¹)	2.403	2.443	2.698	2.780
<i>F</i> (000)	794.0	860.0	3488.0	864.0
Collected reflections	12830	15870	22897	17546
Independent reflections	6705	7993	13900	6897
<i>R</i> _{int}	0.0273	0.0387	0.0824	0.0393
<i>R</i> ₁ [<i>I</i> > 2σ(<i>I</i>)]	0.0341	0.0471	0.0843	0.0309
w <i>R</i> ₂ (all data)	0.0733	0.0939	0.1959	0.0648
Goodness of fit on <i>F</i> ²	1.020	1.009	0.987	1.011
CCDC numbers	1542700	1542701	1542702	1542703

a) $R_1 = \sum |Fo| - |Fc| / \sum |Fo|$. b) $wR_2 = \sqrt{\sum [w(Fo^2 - Fc^2)^2] / \sum [w(Fo^2)^2]}$.**Table S2.** Dy(III) Geometry Analysis by SHAPE Software.

		ideal geometries	S
Complex 1	Dy1	Biaugmented trigonal prism (C _{2v})	1.929
		Triangular dodecahedron (D _{2d})	2.498
		Square antiprism (D _{4d})	3.316
	Dy1'	Biaugmented trigonal prism (C _{2v})	1.929
		Triangular dodecahedron (D _{2d})	2.498
		Square antiprism (D _{4d})	3.316
	Ca	Octahedron (O _h)	4.265
		Trigonal prism (D _{3h})	14.466
		Hexagon (D _{6h})	27.158
Complex 2	Dy1	Triangular dodecahedron (D _{2d})	2.437
		Biaugmented trigonal prism (C _{2v})	2.494
		Square antiprism (D _{4d})	3.648
	Dy1'	Triangular dodecahedron (D _{2d})	2.483
		Biaugmented trigonal prism (C _{2v})	2.496
		Square antiprism (D _{4d})	3.648
	Mg	Octahedron (O _h)	2.011
		Trigonal prism (D _{3h})	14.470
		Hexagon (D _{6h})	28.386
Complex 3	Er1	Biaugmented trigonal prism (C _{2v})	1.893
		Triangular dodecahedron (D _{2d})	1.950
		Square antiprism (D _{4d})	2.252
	Er1'	Biaugmented trigonal prism (C _{2v})	1.893
		Triangular dodecahedron (D _{2d})	1.950
		Square antiprism (D _{4d})	2.252

	Ca1	Octahedron (O_h)	4.273
		Trigonal prism (D_{3h})	14.527
		Hexagon (D_{6h})	26.812
	Er2	Triangular dodecahedron (D_{2d})	1.468
		Biaugmented trigonal prism (C_{2v})	2.484
		Square antiprism (D_{4d})	2.571
	Er2'	Triangular dodecahedron (D_{2d})	1.468
		Biaugmented trigonal prism (C_{2v})	2.484
		Square antiprism (D_{4d})	2.571
	Ca2	Octahedron (O_h)	4.547
		Trigonal prism (D_{3h})	14.535
		Hexagon (D_{6h})	27.207
Complex 4	Er1	Triangular dodecahedron (D_{2d})	2.276
		Biaugmented trigonal prism (C_{2v})	2.293
		Square antiprism (D_{4d})	3.405
	Er1'	Triangular dodecahedron (D_{2d})	2.276
		Biaugmented trigonal prism (C_{2v})	2.293
		Square antiprism (D_{4d})	3.405
	Mg	Octahedron (O_h)	2.008
		Trigonal prism (D_{3h})	14.479
		Hexagon (D_{6h})	28.437

Table S3. Selected Bond Distances (Å) for **1-4**.

	1	2	3	4			
Dy1-O1	2.251(3)	Dy1-O1	2.267(3)	Er1-O1	2.237(10)	Er1-O1	2.258(2)
Dy1-O3	2.336(3)	Dy1-O4	2.307(3)	Er1-O3	2.312(10)	Er1-O3	2.327(2)
Dy1-O4'	2.339(2)	Dy1-O2	2.343(3)	Er1-O4	2.347(10)	Er1-O4	2.289(2)
Dy1-O2	2.346(2)	Dy1-O3	2.346(3)	Er1-O2	2.309(11)	Er1-O2	2.330(2)
Dy1-N4'	2.512(4)	Dy1-N1	2.497(4)	Er1-N4	2.483(16)	Er1-N1	2.470(3)
Dy1-N1	2.511(4)	Dy1-N2	2.520(4)	Er1-N1	2.466(12)	Er1-N4	2.514(3)
Dy1-N3	2.536(4)	Dy1-N3	2.521(4)	Er1-N3	2.517(11)	Er1-N3	2.488(3)
Dy1-N2	2.539(3)	Dy1-N4	2.539(4)	Er1-N2	2.463(15)	Er1-N2	2.493(3)
Dy1-Ca1	3.4239(2)	Dy1-Mg1	3.1902(4)	Er1-Ca1	3.3871(7)	Er1-Mg1	3.1667(2)
Ca1-O4	2.317(2)	Mg1-O3	2.072(3)	Ca1-O4	2.298(12)	Mg1-O4	2.053(2)
Ca1-O4'	2.317(2)	Mg1-O4	2.065(3)	Ca1-O4'	2.298(12)	Mg1-O4'	2.053(2)
Ca1-O2'	2.320(2)	Mg1-O2	2.116(3)	Ca1-O2'	2.355(10)	Mg1-O2	2.109(2)
Ca1-O2	2.320(2)	Mg1-O4'	2.065(3)	Ca1-O2	2.355(10)	Mg1-O2'	2.109(2)
Ca1-O3'	2.359(2)	Mg1-O3'	2.072(3)	Ca1-O3'	2.260(8)	Mg1-O3'	2.066(2)
Ca1-O3	2.359(2)	Mg1-O2'	2.116(3)	Ca1-O3	2.260(8)	Mg1-O3	2.066(2)
Ca1-Dy1'	3.4239(2)	Mg1-Dy1'	3.1902(4)	Ca1-Er1'	3.3870(7)	Mg1-Er1'	3.1667(2)
O4-Dy1'	2.339(2)			Er2-O5	2.238(10)		
N4-Dy1'	2.512(4)			Er2-O8	2.289(9)		
				Er2-O6	2.303(10)		
				Er2-O7	2.324(9)		
				Er2-N5	2.463(11)		

	Er2-N6	2.492(13)
	Er2-N7	2.495(13)
	Er2-N8	2.531(11)
	Er2-Ca2	3.3951(7)
	Ca2-O7	2.305(10)
	Ca2-O7'	2.306(10)
	Ca2-O8'	2.330(8)
	Ca2-O8	2.330(8)
	Ca2-O6'	2.381(9)
	Ca2-O6	2.381(9)
	Ca2-Er2'	3.3951(7)

Table S4. Best fitted parameters (χ_T , χ_s , τ and α) with the extended Debye model for complex **1** at 0 Oe in the temperature range 4-11 K.

T/ K	$\chi_s / \text{cm}^3 \text{ mol}^{-1}$	$\chi_T / \text{cm}^3 \text{ mol}^{-1}$	τ/s	α
4	0.24793	7.90061	0.07836	0.20522
4.5	0.19823	6.90022	0.03845	0.18766
5	0.17319	6.10402	0.02046	0.16865
5.5	0.21624	5.10000	0.01029	0.09547
6	0.23955	4.83016	0.00675	0.10190
6.5	0.15042	4.41106	0.00417	0.10328
7	0.13596	4.08285	0.00273	0.09574
7.5	0.12839	3.79893	0.00184	0.08995
8	0.11008	3.55712	0.00128	0.08794
8.5	0.21898	3.34500	0.00093	0.06210
9	0.12109	3.15182	0.00065	0.07679
9.5	0.12789	2.98052	0.00048	0.07270
10	0.20704	2.82928	0.00037	0.06006
10.5	0.22374	2.69238	0.00028	0.05956
11	0.17078	2.56296	0.00020	0.07060

Table S5. Best fitted parameters (χ_T , χ_s , τ and α) with the extended Debye model for complex **2** at 0 Oe in the temperature range 4-13 K.

T/ K	$\chi_s / \text{cm}^3 \text{ mol}^{-1}$	$\chi_T / \text{cm}^3 \text{ mol}^{-1}$	τ/s	α
4	0.26470	13.90011	0.06731	0.11132
5	0.22450	10.40466	0.01962	0.07461
6	0.14963	8.70036	0.00789	0.08169
7	0.12237	7.40022	0.00372	0.08006
8	0.29066	6.40002	0.00204	0.05306
9	0.26545	5.64400	0.00120	0.04916
10	0.25724	5.06919	0.00076	0.05073
11	0.29344	4.58406	0.00051	0.04679
12	0.24144	4.19033	0.00035	0.05412
13	0.29993	3.85254	0.00024	0.04801

Table S6. The curves are fitted by the modified Arrhenius relationship the Raman process is taken account

$$1/\tau = CT^n + \tau_0^{-1} \exp(-U_{\text{eff}}/k_B T)$$

complex	C ($s^{-1} \cdot K^{-n}$)	n	τ_0 (s)	U_{eff}/k_B (K)
1	0.005	5.7	2.9×10^{-6}	67.0
2	0.05	4.0	1.7×10^{-5}	41.0

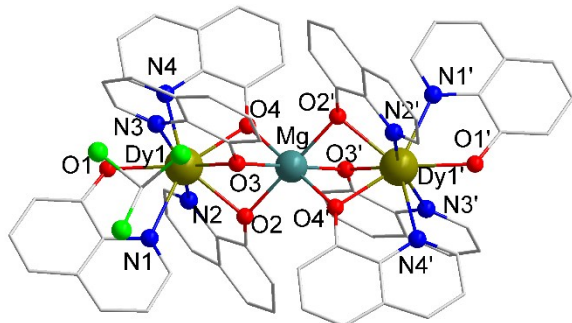


Fig. S1 The crystal structure of complex **2** (hydrogen atoms are omitted for clarity).

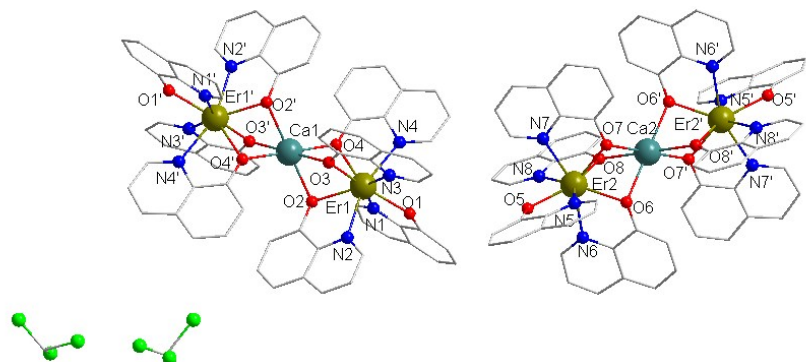


Fig. S2 The crystal structure of complex **3** (hydrogen atoms are omitted for clarity).

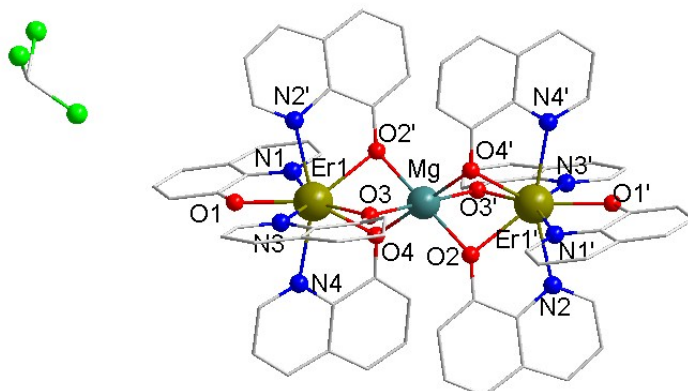


Fig. S3 The crystal structure of complex **4** (hydrogen atoms are omitted for clarity).

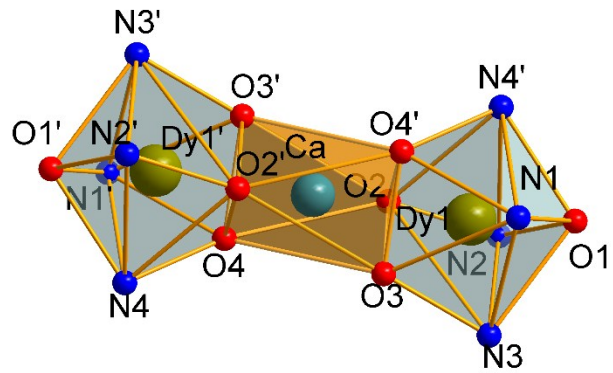


Fig. S4 The local coordination geometry of the Dy(III) ions and Ca(II) ion in complex **1**.

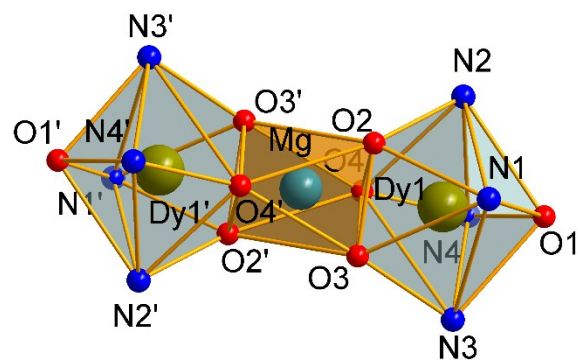


Fig. S5 The local coordination geometry of the Dy(III) ions and Mg(II) ion in complex **2**.

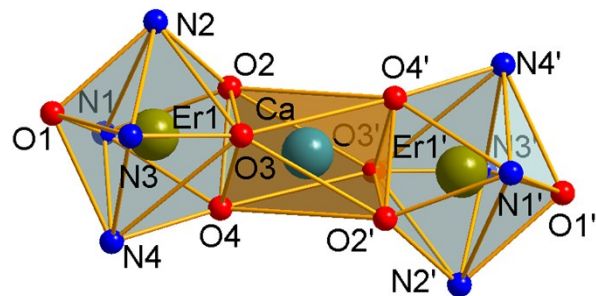


Fig. S6 The local coordination geometry of the Dy(III) ions and Mg(II) ion in complex **3**.

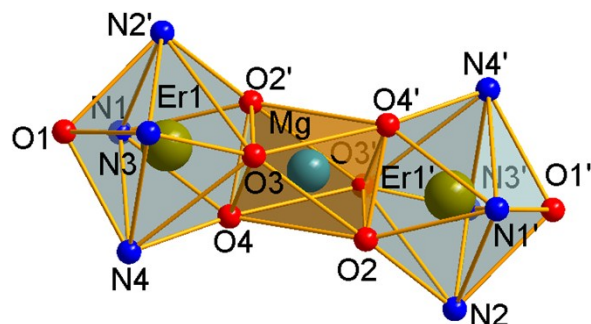


Fig. S7 The local coordination geometry of the Dy(III) ions and Mg(II) ion in complex **4**.

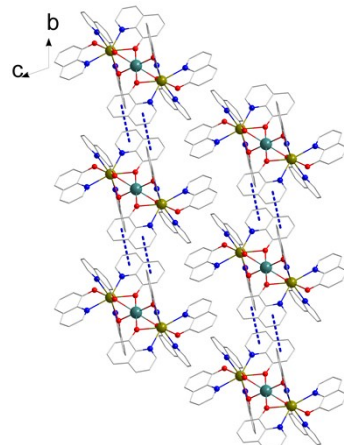


Fig. S8 Crystal packing of **2** along the *a*-axis.

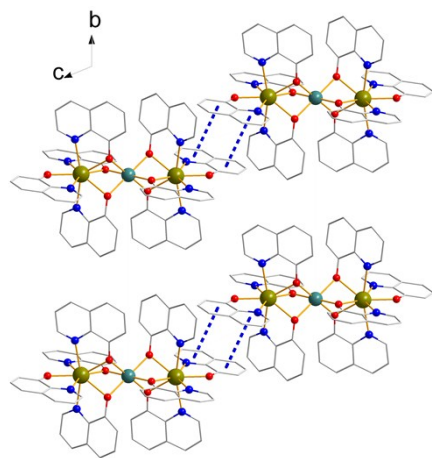


Fig. S9 Crystal packing of **2** along the *a*-axis.

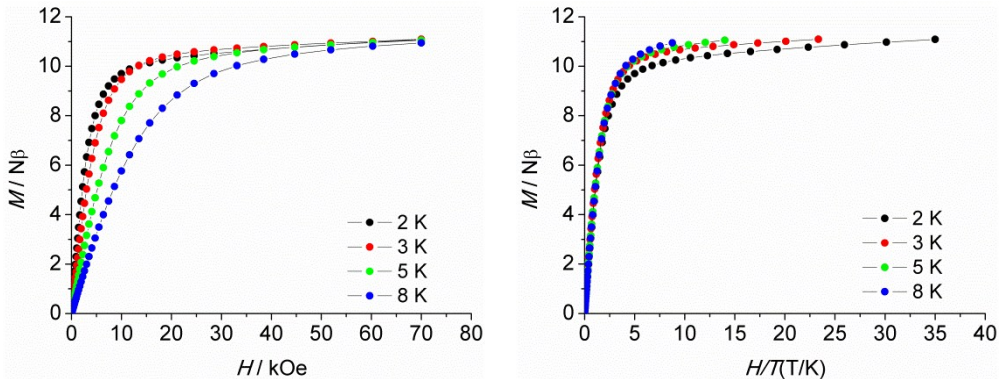


Fig. S10 The field dependence of magnetization (left) and magnetization data (right) for **1** at 2, 3, 5 and 8 K.

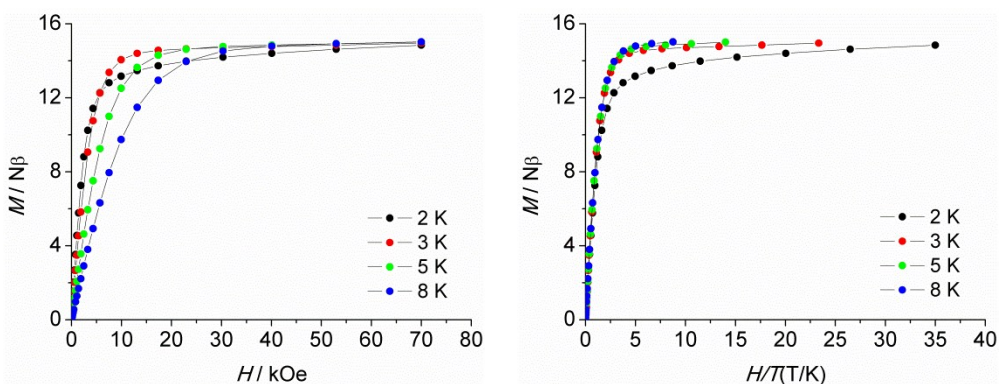


Fig. S11 The field dependence of magnetization (left) and magnetization data (right) for **2** at 2, 3, 5 and 8 K.

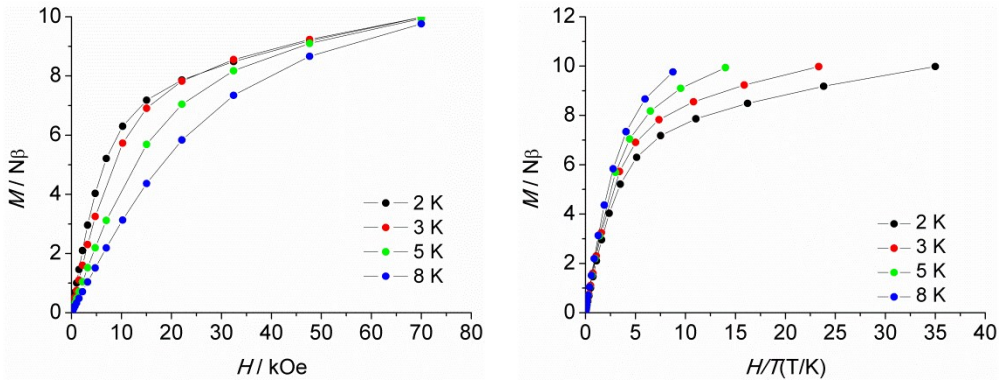


Fig. S12 The field dependence of magnetization (left) and magnetization data (right) for **3** at 2, 3, 5 and 8 K.

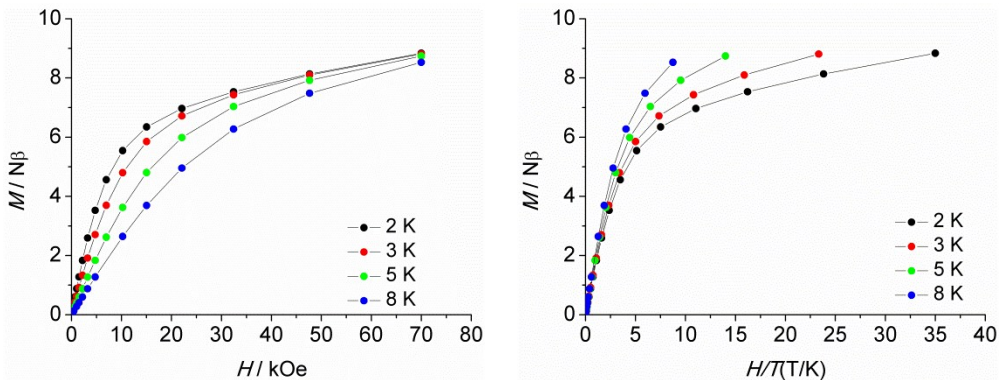


Fig. S13 The field dependence of magnetization (left) and magnetization data (right) for **4** at 2, 3, 5 and 8 K.

With the known isotropic interaction, the Hamiltonian $H = \frac{2J}{N} S_{\text{Gd}1} \cdot S_{\text{Gd}2}$ results in the formula for the temperature dependence of the molar magnetic susceptibility in eqn (S1)^{S1,2}, where g is the Landé factor, β is the Bohr magneton, N is the Avogadro number, and k is the Boltzmann constant and $x = -J/kT$.

$$\chi_M T = \frac{2N g^2 \mu_B^2 e^x + 5e^{3x} + 14e^{6x} + 30e^{10x} + 55e^{15x} + 91e^{21x} + 140e^{28x}}{k(1 + 3e^x + 5e^{3x} + 7e^{6x} + 9e^{10x} + 11e^{15x} + 13e^{21x} + 15e^{28x})} \quad (\text{S1})$$

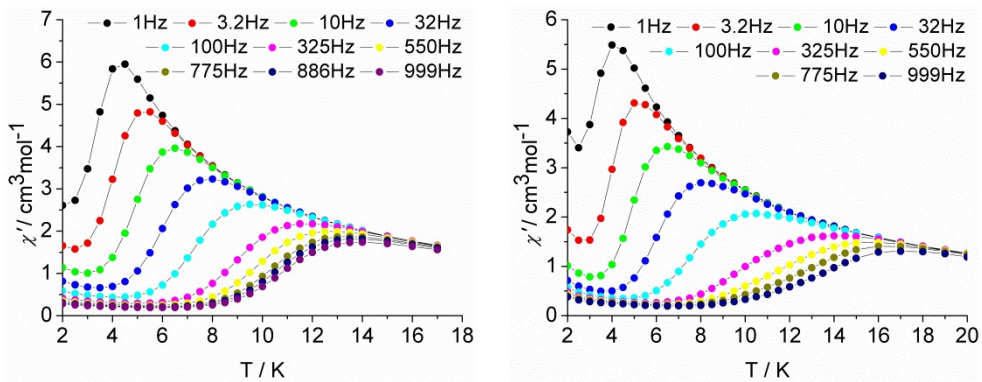


Fig. S14 Plots of the temperature dependent in-phase ac susceptibility (χ') under zero field for **1**(left) and **2**(right).

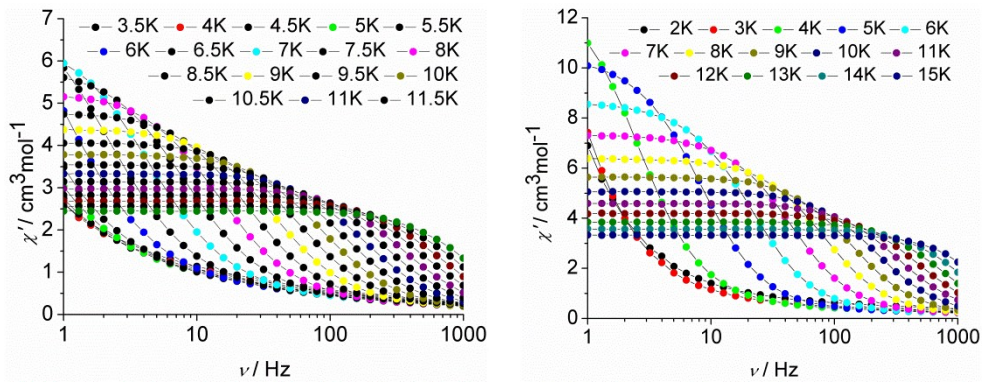


Fig. S15 Plots of the frequency dependent in-phase ac susceptibility (χ') under zero field for **1**(left) and **2**(right).

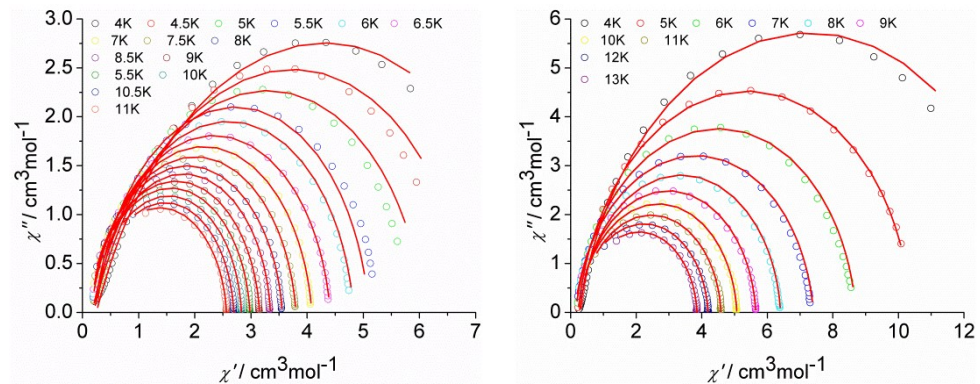


Fig. S16 Cole-Cole plots for **1** (left) and **2** (left) under zero field. The red solid lines represent the best fits.

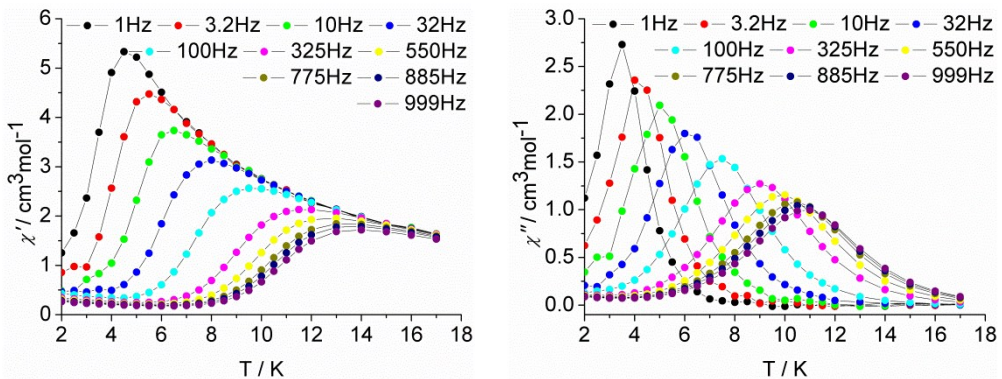


Fig. S17 Plots of the temperature dependent in-phase (χ') and out-of-phase ac susceptibility (χ'') under 1500 Oe field for **1**.

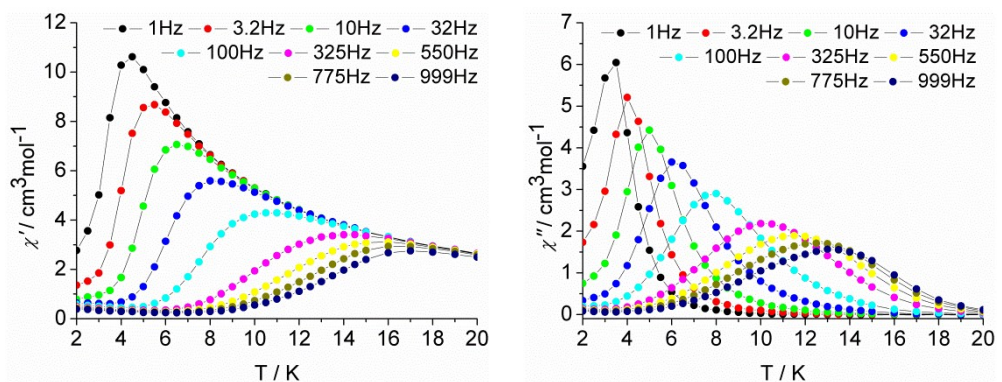


Fig. S18 Plots of the temperature dependent in-phase (χ') and out-of-phase ac susceptibility (χ'') under 1500 Oe field for **2**.

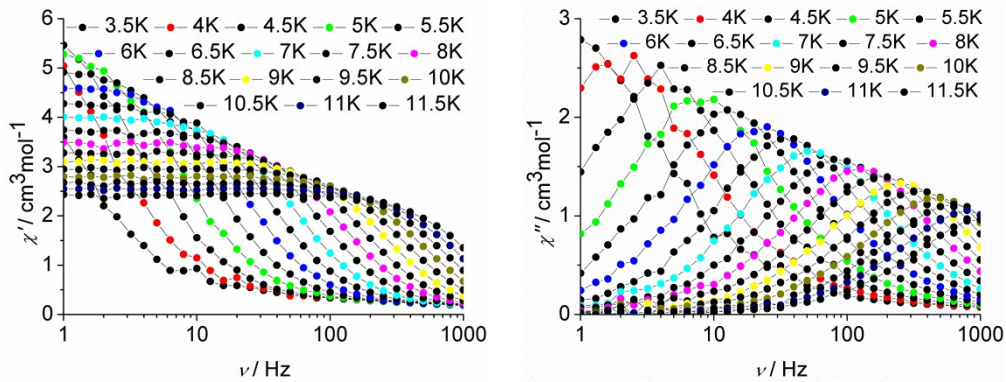


Fig. S19 Plots of the frequency dependent in-phase (χ') and out-of-phase ac susceptibility (χ'') under 1500 Oe field for **1**.

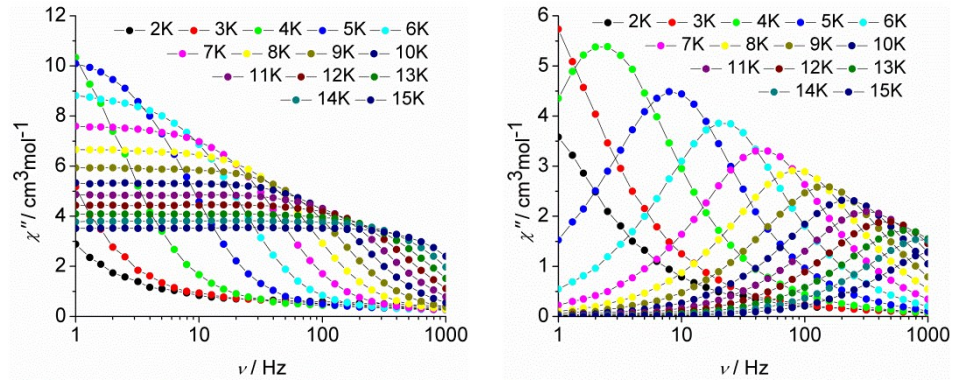


Fig. S20 Plots of the frequency dependent in-phase (χ') and out-of-phase ac susceptibility (χ'') under 1500 Oe field for **1**.

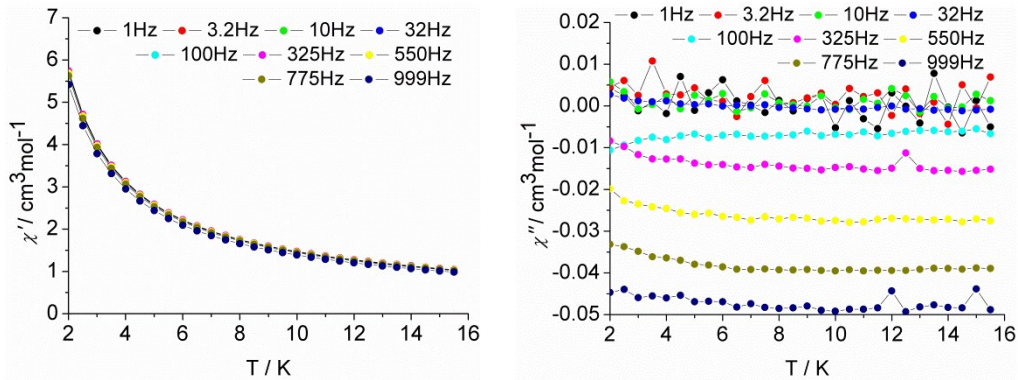


Fig. S21 Plots of the temperature dependent in-phase (χ') and out-of-phase ac susceptibility (χ'') under 0 Oe field for **3**.

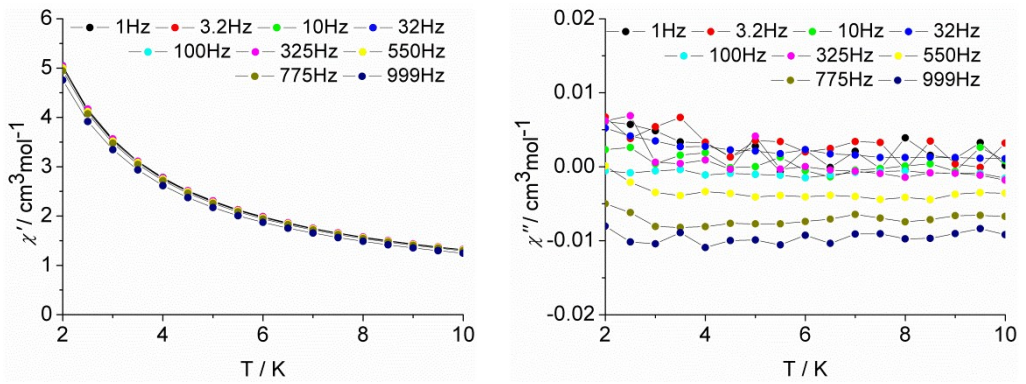


Fig. S22 Plots of the temperature dependent in-phase (χ') and out-of-phase ac susceptibility (χ'') under 0 Oe field for **4**.

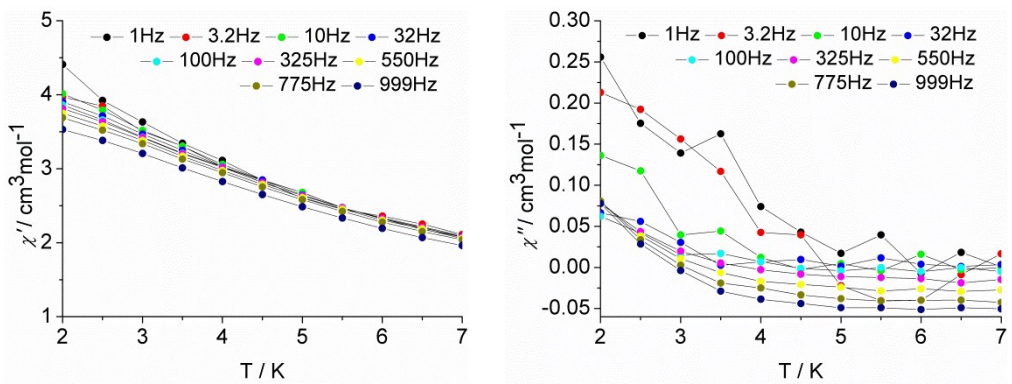


Fig. S23 Plots of the temperature dependent in-phase (χ') and out-of-phase ac susceptibility (χ'') under 3500 Oe field for **3**.

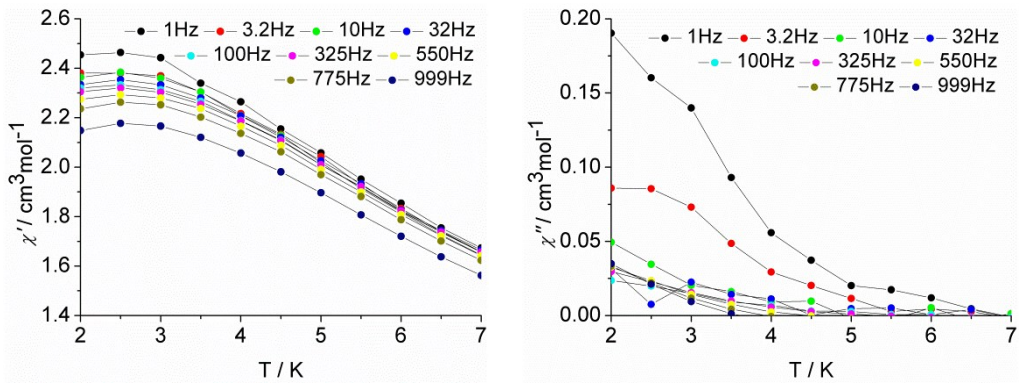


Fig. S24 Plots of the temperature dependent in-phase (χ') and out-of-phase ac susceptibility (χ'') under 5000 Oe field for **4**.

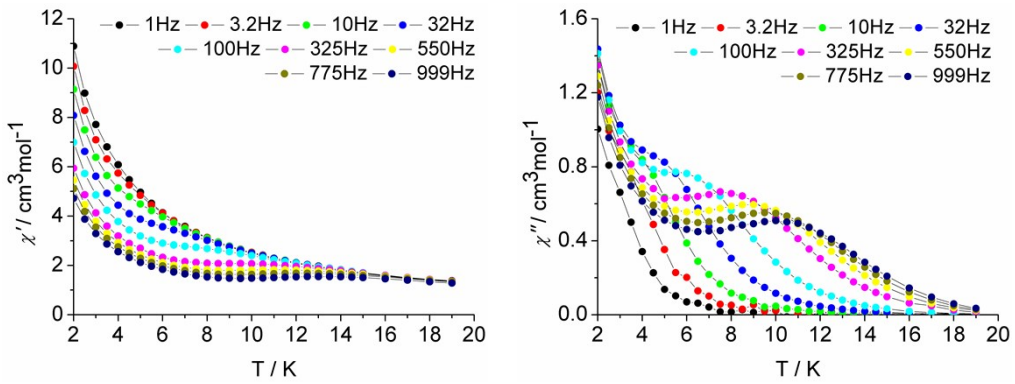


Fig. S25 Plots of the temperature dependent in-phase (χ') and out-of-phase ac susceptibility (χ'') under 0 Oe field for **1a**.

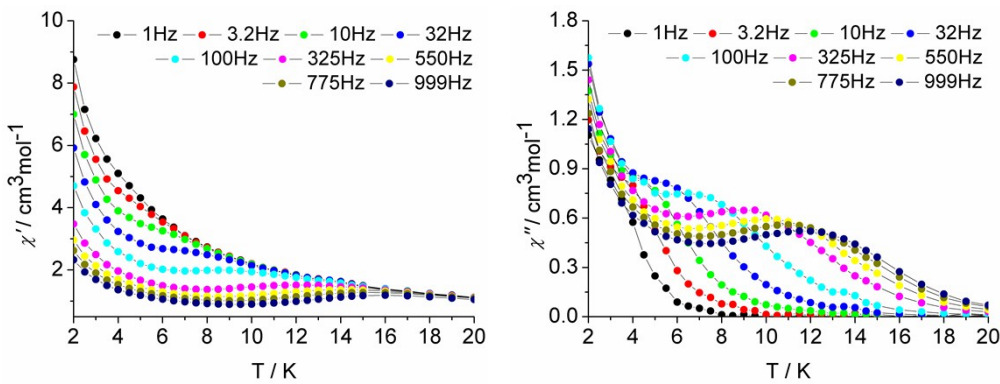


Fig. S26 Plots of the temperature dependent in-phase (χ') and out-of-phase ac susceptibility (χ'') under 0 Oe field for **2a**.

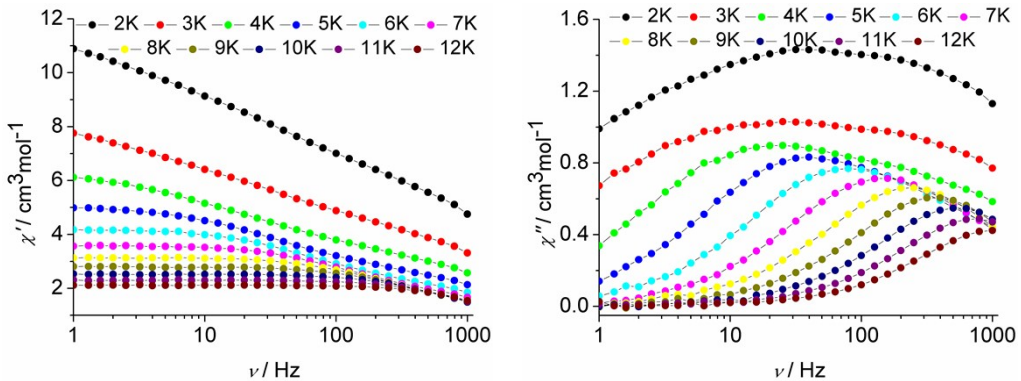


Fig. S27 Plots of the frequency dependent in-phase (χ') and out-of-phase ac susceptibility (χ'') under 0 Oe field for **1a**.

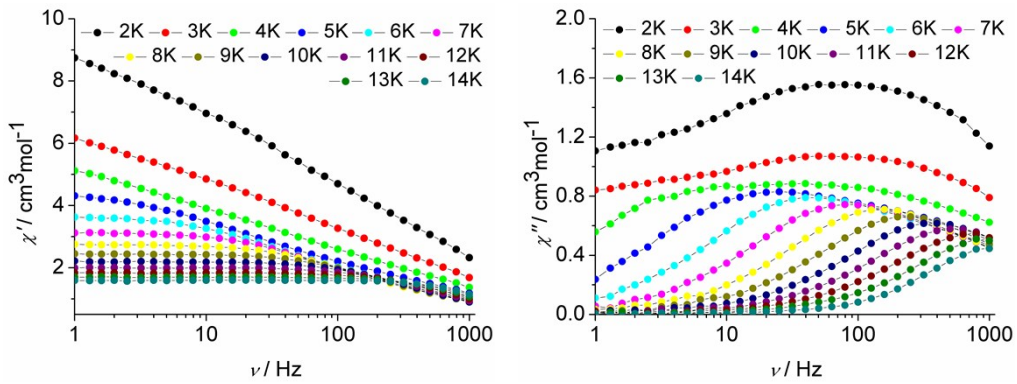


Fig. S28 Plots of the frequency dependent in-phase (χ') and out-of-phase ac susceptibility (χ'') under 0 Oe field for **2a**.

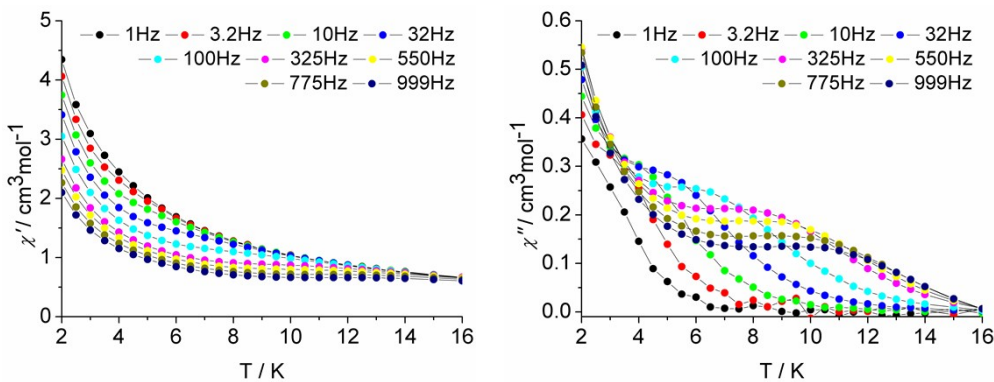


Fig. S29 Plots of the temperature dependent in-phase (χ') and out-of-phase ac susceptibility (χ'') under 0 Oe field for **1b**.

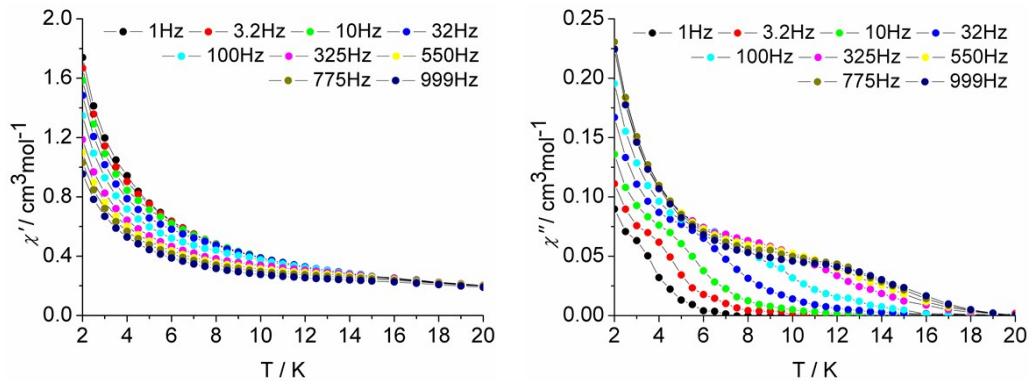


Fig. S30 Plots of the temperature dependent in-phase (χ') and out-of-phase ac susceptibility (χ'') under 0 Oe field for **2b**.

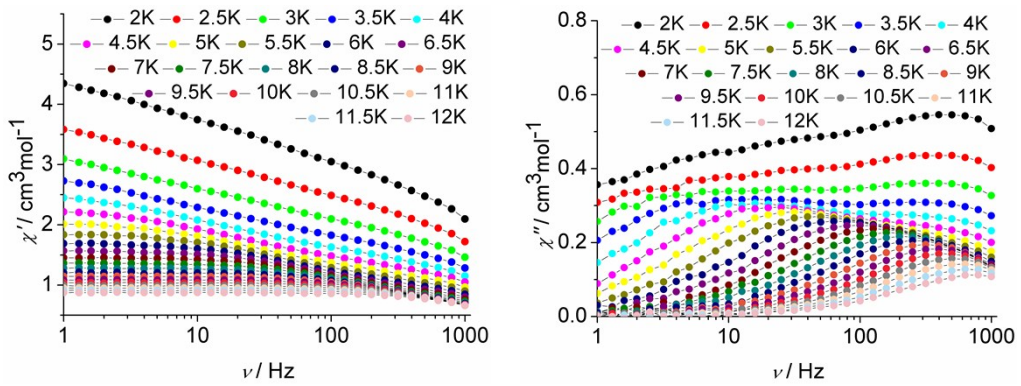


Fig. S31 Plots of the frequency dependent in-phase (χ') and out-of-phase ac susceptibility (χ'') under 0 Oe field for **1b**.

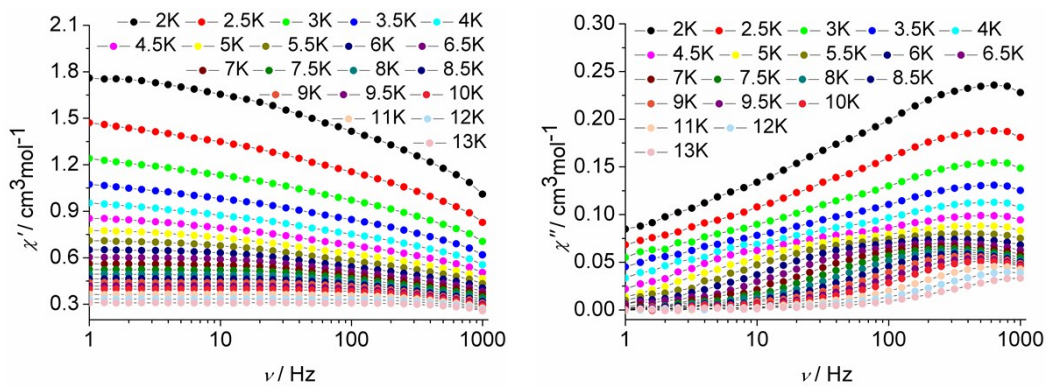


Fig. S32 Plots of the frequency dependent in-phase (χ') and out-of-phase ac susceptibility (χ'') under 0 Oe field for **2b**.

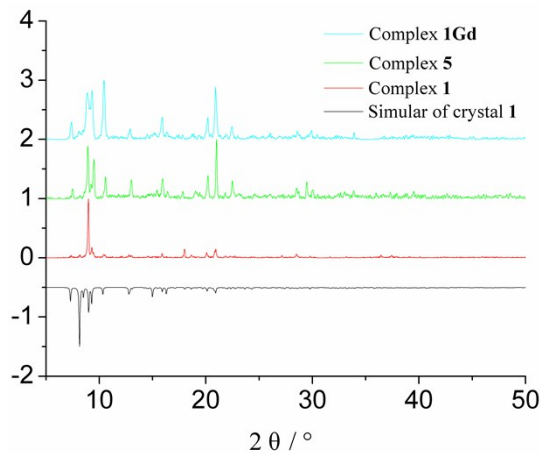


Fig. S33 PXRD patterns for complexes **1**, **5** and **1Gd**.

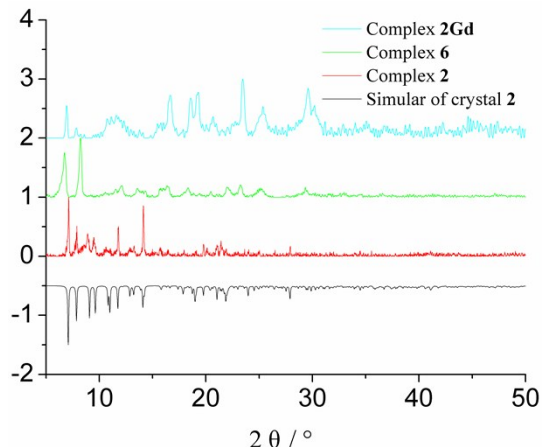


Fig. S34 PXRD patterns for complexes **2**, **6** and **2Gd**.

Computational details

The dinuclear complexes **1-2** have an inversion center, thus only one magnetic center is calculated. Complete-active-space self-consistent field (CASSCF) calculations on individual lanthanide Dy(III) fragment of the complete structure (see Fig. S35 for the complete structures of complexes **1-2**) on the basis of single-crystal X-ray determined geometry have been carried out with MOLCAS 8.0 program package.^{S3} Each dysprosium center was calculated keeping the experimentally determined structure of the corresponding complex while replacing the neighboring Dy(III) ion by diamagnetic Lu(III).

The basis sets for all atoms are atomic natural orbitals from the MOLCAS ANO-RCC library: ANO-RCC-VTZP for Dy(III) ions; VTZ for close O and N; VDZ for distant atoms. The calculations employed the second order Douglas-Kroll-Hess Hamiltonian, where scalar relativistic contractions were taken into account in the basis set and the spin-orbit couplings were handled separately in the restricted active space state interaction (RASSI-SO) procedure. For the fragment of Dy(III), active electrons in 7 active spaces include all f electrons CAS(9 in 7) in the CASSCF calculation. We have mixed the maximum number of spin-free state which was possible with our hardware (all from 21 sextets, 128 from 224 quadruplets, 130 from 490 doublets for the Dy(III) fragment).

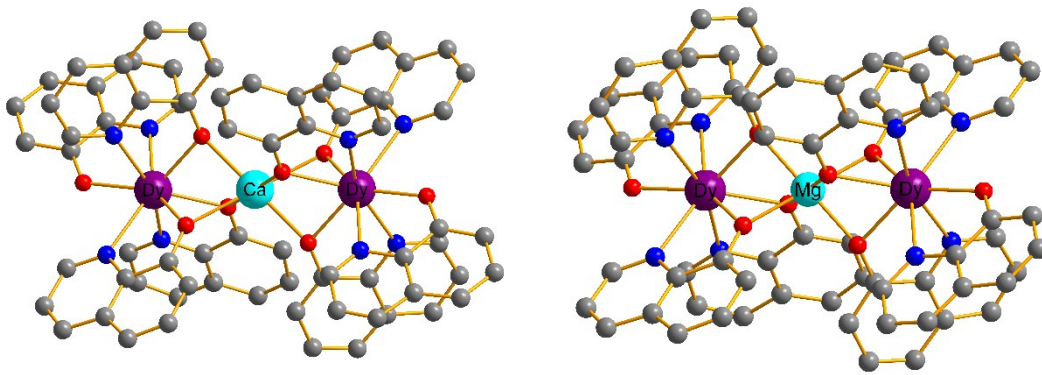


Fig. S35 Calculated structures for complexes **1** (left) and **2** (right).

To fit the exchange interactions in these complexes, we took two steps to obtain them.

Firstly, we calculated one Dy(III) fragment using CASSCF to obtain the corresponding magnetic properties. Then, the exchange interaction between the magnetic centers is considered within the Lines model,^{S4} while the account of the dipole-dipole magnetic coupling is treated exactly. The Lines model is effective and has been successfully used widely in the research field of f-element single-molecule magnets.^{S5}

For each of complexes **1-2**, there is only one type of J .

The exchange Hamiltonian is:

$$\hat{H}_{exch} = -J_{total} \hat{\mathcal{S}}_{Dy1}^z \hat{\mathcal{S}}_{Dy1A}^z \quad (\text{S1})$$

The J_{total} is the parameter of the total magnetic interaction ($J_{total} = J_{dipolar} + J_{exchange}$) between magnetic center ions. The $\hat{\mathcal{S}}_{Dy}^z = \pm 1/2$ are the ground pseudospin on the Dy(III) sites. The dipolar magnetic coupling can be calculated exactly, while the exchange coupling constants were fitted through comparison of the computed and measured magnetic susceptibility and molar magnetization using the POLY_ANISO program.^{S6}

Table S7. Calculated energy levels (cm^{-1}), g (g_x, g_y, g_z) tensors and m_J values of the lowest Kramers doublets (KDs) of one Dy center for complexes **1-2**.

KD	1			2		
	E/cm^{-1}	g	m_J	E/cm^{-1}	g	m_J
1	0.0	0.003		0.0	0.007	
		0.007	$\pm 15/2$		0.010	$\pm 15/2$
		19.759			19.747	
2	102.2	0.071		158.1	0.095	
		0.090	$\pm 13/2$		0.099	$\pm 13/2$

		17.008		17.065	
		0.154		0.147	
3	223.8	0.230	$\pm 11/2$	288.8	0.183
		13.806			14.133
		3.119			2.868
4	321.7	3.626	$\pm 9/2$	383.7	3.402
		10.227			10.246
		7.983			8.010
5	396.5	6.624	$\pm 3/2$	457.3	6.172
		1.483			1.752
		2.362			2.625
6	454.2	3.623	$\pm 1/2$	531.3	3.223
		12.033			12.980
		0.463			0.431
7	538.3	1.077	$\pm 5/2$	642.8	1.265
		17.914			16.949
		0.082			0.398
8	649.6	0.183	$\pm 7/2$	691.1	1.601
		19.545			18.332

Table S8. Exchange energies (cm^{-1}) and main values of the g_z for the lowest two exchange doublets of **1-2**.

	1		2	
	<i>E</i>	<i>g_z</i>	<i>E</i>	<i>g_z</i>
1	0.0	39.518	0.0	39.494
2	3.5	0.000	2.3	0.000

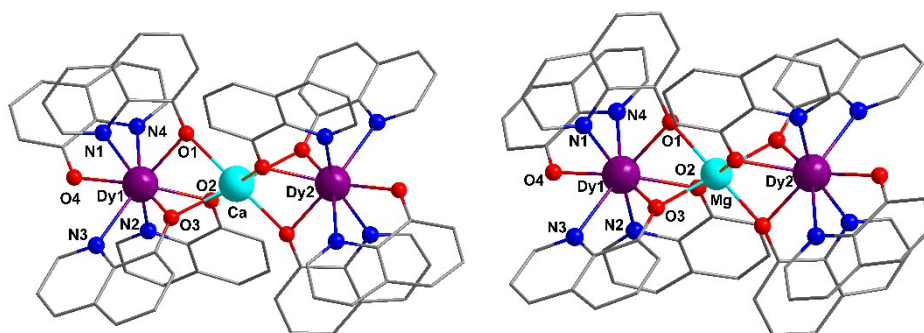


Fig. S36 Labeled molecular structures of complexes **1** (left) and **2** (right).

Table S9. Natural Bond Order (NBO) charges per atoms in the ground state of complexes **1-2** calculated within CASSCF

	1	2
Dy1	2.482	2.480
Ca	1.763	
Mg		1.654
O1	-0.922	-0.907
O2	-0.929	-0.907

O3	-0.914	-0.910
O4	-0.878	-0.908
N1	-0.372	-0.355
N2	-0.350	-0.369
N3	-0.359	-0.364
N4	-0.348	-0.369

References:

- S1 W. Plass, G. Fries, Z. Anorg, *Allg. Chem.*, 1997, **623**, 1205.
- S2 P. Comba, M. Großhauser, R. Klingeler, C. Koo, Y. Lan, D. Müller, J. Park, A. Powell, M. J. Riley, H. Wadeohl, *Inorg. Chem.*, 2015, **54**, 11247.
- S3 G. Karlström, R. Lindh, P.-Å. Malmqvist, B. O. Roos, U. Ryde, V. Veryazov, P.-O. Widmark, M. Cossi, B. Schimmelpfennig, P. Neogrády and L. Seijo, MOLCAS: a Program Package for Computational Chemistry. *Comput. Mater. Sci.*, 2003, **28**, 222.
- S4 M. E. Lines, *J. Chem. Phys.*, 1971, **55**, 2977.
- S5 (a) K. C. Mondal, A. Sundt, Y. H. Lan, G. E. Kostakis, O. Waldmann, L. Ungur, L. F. Chibotaru, C. E. Anson and A. K. Powell, *Angew. Chem. Int. Ed.*, 2012, **51**, 7550. (b) S. K. Langley, D. P. Wielechowski, V. Vieru, N. F. Chilton, B. Moubaraki, B. F. Abrahams, L. F. Chibotaru and K. S. Murray, *Angew. Chem. Int. Ed.*, 2013, **52**, 12014.
- S6 (a) L. F. Chibotaru, L. Ungur, A. Soncini, *Angew. Chem. Int. Ed.*, 2008, **47**, 4126. (b) L. Ungur, W. Van denHeuvel and L.F. Chibotaru, *New J. Chem.*, 2009, **33**, 1224. (c) L. F. Chibotaru, L. Ungur, C. Aronica, H. Elmoll, G. Pilet and D. Luneau, *J. Am. Chem. Soc.*, 2008, **130**, 12445.